

# Laser-Doppler Velocimetry: Analytical Solution of the Optical System Including the Effects of Partial Coherence of the Source

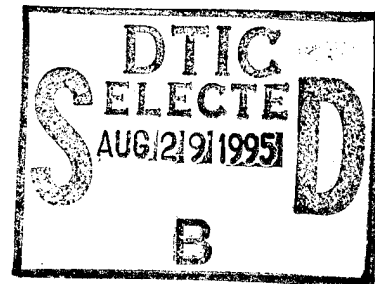
15 January 1995

19950828 011

Prepared by

H. T. YURA  
Electronics Technology Center  
Technology Operations

S. G. HANSON and L. LADING  
Risø National Laboratory  
Roskilde, Denmark



Prepared for

SPACE AND MISSILE SYSTEMS CENTER  
AIR FORCE MATERIEL COMMAND  
2430 E. El Segundo Boulevard  
Los Angeles Air Force Base, CA 90245

Engineering and Technology Group

This report was submitted by The Aerospace Corporation, El Segundo, CA 90245-4691, under Contract No. F04701-93-C-0094 with the Space and Missile Systems Center, 2430 E. El Segundo Blvd., Los Angeles Air Force Base, CA 90245. It was reviewed and approved for The Aerospace Corporation by T. A. Galantowicz, Principal Director, Electronics Technology Center. Col. Charles E. Whited was the project officer for the program.

This report has been reviewed by the Public Affairs Office (PAS) and is releasable to the National Technical Information Service (NTIS). At NTIS, it will be available to the general public, including foreign nationals.

This technical report has been reviewed and is approved for publication. Publication of this report does not constitute Air Force approval of the report's findings or conclusions. It is published only for the exchange and stimulation of ideas.



---

Charles E. Whited, Col. USAF  
SMC/SD

<b>REPORT DOCUMENTATION PAGE</b>			Form Approved OMB No. 0704-0188	
Public reporting burden for this collection of information is estimated to average 1 hour per response, including the time for reviewing instructions, searching existing data sources, gathering and maintaining the data needed, and completing and reviewing the collection of information. Send comments regarding this burden estimate or any other aspect of this collection of information, including suggestions for reducing this burden to Washington Headquarters Services, Directorate for Information Operations and Reports, 1215 Jefferson Davis Highway, Suite 1204, Arlington, VA 22202-4302, and to the Office of Management and Budget, Paperwork Reduction Project (0704-0188), Washington, DC 20503.				
1. AGENCY USE ONLY (Leave blank)		2. REPORT DATE 15 January 1995		3. REPORT TYPE AND DATES COVERED
4. TITLE AND SUBTITLE Laser-Doppler Velocimetry: Analytical Solutions of the Optical System Including the Effects of Partial Coherence of the Source			5. FUNDING NUMBERS  F04701-93-C-0094	
6. AUTHOR(S) H. T. Yura, S. G. Hanson, and L. Lading				
7. PERFORMING ORGANIZATION NAME(S) AND ADDRESS(ES) The Aerospace Corporation Technology Operations El Segundo, CA 90245-4691			8. PERFORMING ORGANIZATION REPORT NUMBER  TR-95(5925)-3	
9. SPONSORING/MONITORING AGENCY NAME(S) AND ADDRESS(ES) Space and Missile Systems Center Air Force Materiel Command 2430 E. El Segundo Boulevard Los Angeles Air Force Base, CA 90245			10. SPONSORING/MONITORING AGENCY REPORT NUMBER  SMC-TR-95-29	
11. SUPPLEMENTARY NOTES				
12a. DISTRIBUTION/AVAILABILITY STATEMENT  Approved for public release; distribution unlimited			12b. DISTRIBUTION CODE	
13. ABSTRACT (Maximum 200 words)  Within the framework of ABCD matrix theory, analytical expressions are derived for the time-lagged covariance of a classical laser Doppler velocimetry system as a function of the laser spot size, the limiting aperture, and the measurement aperture size. Both partial and fully developed speckle are considered, as well as planar and rotating targets. Further, error estimates are presented that indicate how well one can determine the velocity, in practice, of both planar and rotating targets, and a comparison with time-of flight velocimetry is given.				
14. SUBJECT TERMS  ABCD ray matrix theory, Doppler velocimetry, Laser speckle			15. NUMBER OF PAGES 23	
			16. PRICE CODE	
17. SECURITY CLASSIFICATION OF REPORT UNCLASSIFIED	18. SECURITY CLASSIFICATION OF THIS PAGE UNCLASSIFIED	19. SECURITY CLASSIFICATION OF ABSTRACT UNCLASSIFIED	20. LIMITATION OF ABSTRACT	

## Preface

The work was partly supported by the Danish Council for Technological Development and by DANTEC Measurement Technology A/S. The research of H. T. Yura was performed while he was a guest scientist at the Risø National Laboratory, Roskilde, Denmark, September–November 1994.

Accession For	
NTIS GRA&I	<input checked="checked" type="checkbox"/>
DTIC TAB	<input type="checkbox"/>
Unannounced	<input type="checkbox"/>
Justification	
By	
Distribution	
Availability Codes	
Dist	Avail and/or Special

A-1

## Contents

1. Introduction.....	1
2. Time-Lagged Covariance for LDV Systems.....	3
2.1 Planar Targets.....	6
2.2 Rotating Targets .....	10
3. Error Estimates.....	15
4. Discussion and Conclusion.....	17
References and Footnotes.....	19
Appendix A .....	21
Appendix B.....	23

## Figures

1. Schematic of a Laser Doppler Velocimeter system.....	3
2. Optical diagram for a LDV system.....	5
3. The reflected intensity distribution for $\Lambda = \sigma_s/5$ .....	7
4. Measurement geometry for a rotating cylindrical shaft. ....	11

## Table

1. Minimum Radii of Curvature for Measurement on Cylindrical Surfaces in the Two Limiting Cases for LDV and LTV .....	18
--	----

## 1. Introduction

Laser velocimeters have found widespread use for localized measurements of fluid velocity. The most common system for this application is the so-called laser Doppler anemometer (LDA).<sup>1</sup> We will consider such a system, not for fluid flow measurements, but for measuring the velocity of solid surfaces or objects large compared to any scale defined by the instrument. In cases of solid objects, we use the term laser Doppler *velocimetry* (LDV) rather than anemometry. Light scattering in these cases is often dominated by speckle phenomena. The correlation function and the corresponding power spectrum are evaluated for different types of surface statistics and for different parameters defining the operational mode<sup>2</sup> of the instrument. The present analysis is performed using the method of generalized *ABCD* matrices.<sup>3</sup>

The case of fully developed speckle and a large collection aperture will give a power spectrum of the same type as encountered in laser Doppler anemometry with a large number of particles.<sup>4</sup> The shape of the spectrum is then exclusively determined by the geometry of the measuring system, the optical wavelength, and the velocity of the scattering object. This is in contrast to the situation of partially developed speckle, or in cases of speckle decorrelation. In such cases, the spectral shape and the modulation depth of the signal will depend on both the spatial scales of the surface roughness and on out-of-plane motions. The uncertainty of the estimated velocity has been investigated by Lading and Edwards<sup>5</sup> in cases that correspond to fully developed speckle. Here, we will expand the results so that partially developed speckle and speckle decorrelation are also incorporated in the analysis. We assume that photon/electron noise is negligible.

In Sec. 2, we derive general expressions for the auto covariance of the photodetector current in LDV systems and present closed-form analytical results for planar targets that have rough surfaces such that the reflected optical phase exhibits partial spatial coherence. This is important for measurements on smoother surfaces that do not give rise to fully developed speckle. In Sec. 2.2, we obtain corresponding results for the case of fully developed speckle from curved surfaces, which is important for determining the angular velocity of rotating cylindrical shafts. In Sec. 3, error estimates are derived that indicate how well one can estimate the velocity of both planar and rotating targets in practice. Finally, in Sec. 4, a comparison with time-of-flight velocimetry on similar targets is given.

## 2. Time-Lagged Covariance for LDV Systems

We consider the classical LDV system depicted in Figure 1. Two intersecting laser beams produce on a surface an interference fringe pattern, which is imaged onto a square-law detector. It is assumed here, as indicated in Figure 1, that the x-axis of object-plane coordinates is perpendicular to the interference fringes, and that the z-axis is parallel to the optic-axis. It is also assumed that the spacing between fringes is small compared to the overall laser spot diameter (i.e., the number of observable fringes are much greater than unity). Furthermore, the diffusing target is assumed to move with a constant velocity,  $v$ , that is nearly perpendicular to the z-axis.

We seek to determine the time-lagged (auto) covariance of the resulting photocurrent from the detector centered at the corresponding geometrical-image point of the center of the target spot. This quantity is given by

$$C_i(\tau) = \langle i(t)i(t+\tau) \rangle - \langle i(t) \rangle \langle i(t+\tau) \rangle, \quad (2.1)$$

where  $i(t)$  is the photocurrent obtained from the detector at time  $t$  ( $\tau$  is the time-lag), and angular brackets denote the ensemble average over the realizations of the statistics of the reflected light, assumed here to be stationary.

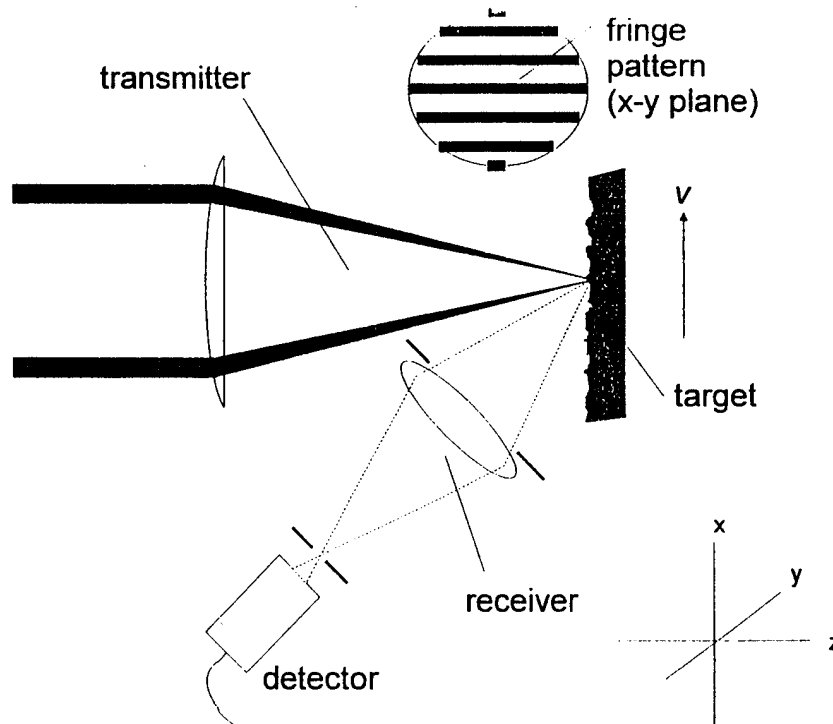


Figure 1. Schematic of a Laser Doppler Velocimeter system. The transmitter and receiver are here shown as separate units. Often they are combined and have a common optical axis.

The instantaneous photocurrent is given by<sup>6</sup>

$$i(t) = \alpha \int d\mathbf{p} W(\mathbf{p}) I(\mathbf{p}, t), \quad (2.2)$$

where  $\mathbf{p}$  is a vector in the image plane,  $I(\mathbf{p}, t)$  is the corresponding image-plane intensity distribution,  $W(\mathbf{p})$  is the receiver-aperture weighting function, and  $\alpha$  is a conversion factor (i.e., power to current) given by

$$\alpha = \frac{q\eta}{h\nu}, \quad (2.3)$$

where  $q$  is the electronic charge,  $\eta$  is the detector quantum efficiency,  $\nu$  is the optical frequency, and  $h$  is Planck's constant. Here we model the (real and positive) receiver aperture weighting function by a circularly symmetric Gaussian-shaped function of the form

$$W(p) = \exp\left[-\frac{2p^2}{\sigma_a^2}\right], \quad (2.4)$$

where  $\sigma_a$  is the  $1/e^2$  radius of the receiver aperture weighting function.

The instantaneous intensity function can be written as

$$I(\mathbf{p}, t) = \left| \int d\mathbf{r} U_o(\mathbf{r}, t) G(\mathbf{r}, \mathbf{p}) \right|^2, \quad (2.5)$$

where we assume that the detector integration time is long compared with the coherence time of the incident laser light, but short compared with the characteristic speckle fluctuation time;  $U_o(\mathbf{r}, t)$  is the reflected optical field in the object plane (assumed here to be in the  $r_x$ - $r_y$  plane); and  $G(\mathbf{r}, \mathbf{p})$  is the Green's function for the circularly symmetric system, given (to within an unimportant phase factor) by

$$G(\mathbf{r}, \mathbf{p}) = -\frac{ik}{2\pi B} \exp\left[-\frac{ik}{2B} (Dp^2 - 2\mathbf{r} \cdot \mathbf{p} + Ar^2)\right], \quad (2.6)$$



where  $A, B$ , and  $D$  are the ray-matrix components of the system.<sup>7</sup> For the imaging system depicted in Figure 2, these quantities are given by

$$A = -f_2 / f_1 = -m, \quad (2.7)$$

$$B = -\frac{2if_1f_2}{k\sigma^2}, \quad (2.8)$$

$$D = -f_1 / f_2 = -1/m, \quad (2.9)$$

where  $\sigma$  is the  $1/e^2$  radius of the imaging system's limiting (Gaussian) aperture,  $k$  is the optical wave number,  $f_1$  and  $f_2$  are indicated in Figure 2, and  $m$  is the geometrical magnification. Substituting Eqs. (2.7)–(2.9) into Eq. (2.6) yields

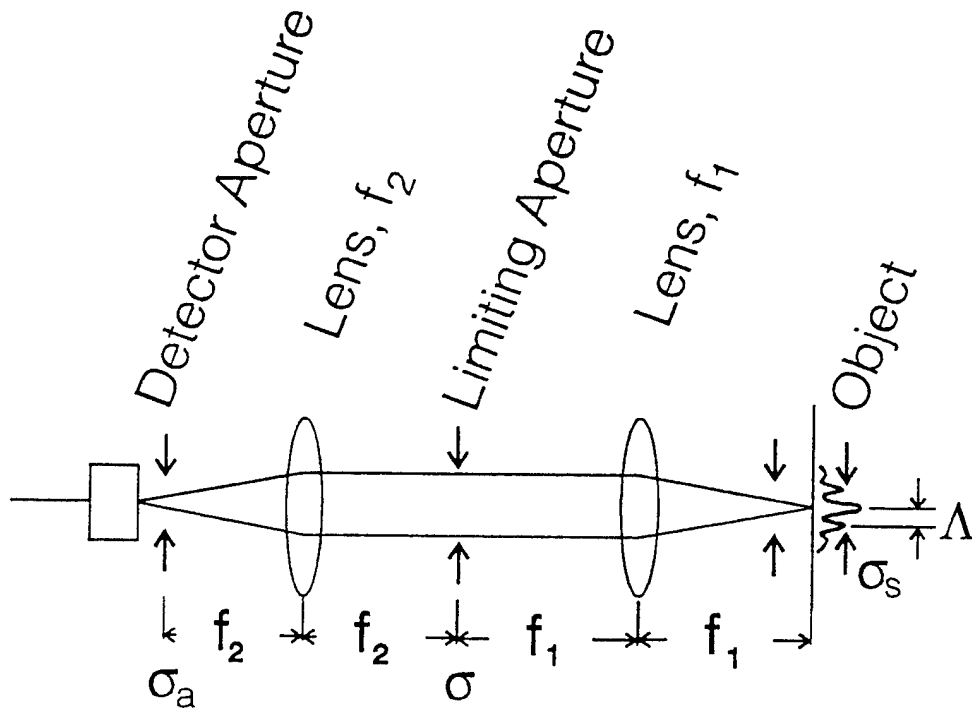


Figure 2. Optical diagram for a LDV system. The limiting aperture of  $1/e^2$  radius  $\sigma$  is positioned in the Fourier plane.

$$G(\mathbf{r}, \mathbf{p}) = (-ik/2\pi B) \exp \left[ -\frac{(\mathbf{x} + \mathbf{r})^2}{\omega^2} \right], \quad (2.10)$$

where

$$\omega = \frac{2f_1}{k\sigma}, \quad (2.11)$$

and

$$\mathbf{x} = \frac{\mathbf{p}}{m}. \quad (2.12)$$

Equation (2.10) expresses the Green's function in terms of object-space variables  $w$  and  $\mathbf{x}$  and is convenient to employ in the ensuing calculations.

## 2.1 Planar Targets

We now assume that the reflected laser interference fringe pattern, which is fixed in space, results from reflection off a partially coherent diffuse planar reflector moving with uniform velocity parallel to the  $r_x$ -axis. In practice, it is a good to assume that the detector aperture is larger than the imaged spot, and, hence, we set  $W(\mathbf{p}) = 1$  in this section. We assume that the amplitude of the reflection coefficient is constant, while the phase exhibits partial spatial coherence. Specifically, we model the reflected optical field for a planar target as

$$U_o(\mathbf{r}, t) = U_i(\mathbf{r})\psi(\mathbf{r}, t), \quad (2.13)$$

where  $U_i(\mathbf{r})$  is the incident field. The mean (diffuse) reflected interference fringe intensity is given by

$$I_o(\mathbf{r}) = |U_i(\mathbf{r})|^2 = \frac{4P_o}{\pi\sigma_s^2} \cos^2(\kappa_x r_x / 2) \exp \left[ -\frac{2r^2}{\sigma_s^2} \right], \quad (2.14)$$

where  $P_o$  is the reflected power,  $\sigma_s$  is the  $1/e^2$  Gaussian spot radius, and

$$\kappa_x = \frac{2\pi}{\Lambda}, \quad (2.15)$$

where  $\Lambda$ , the fringe period, satisfies the condition that  $\Lambda < \sigma_s$  (i.e., many fringes are contained within the reflected spot). As an illustrative example, we plot in Figure 3 the reflected intensity distribution for the case where  $\Lambda = \sigma_s/5$ .

We further assume that  $|\psi(\mathbf{r}, t)| = \rho$ , where  $\rho$  is the magnitude of the reflection coefficient. Here we assume that  $\rho$  is constant and set it equal to unity in the following. As discussed in Appendix A, the correlation function  $B_\psi \equiv \langle \psi(\mathbf{r}_1, t) \psi^*(\mathbf{r}_2, t) \rangle$  is modeled by a Gaussian function given by

$$B_\psi(\mathbf{r}_1, \mathbf{r}_2) = \left( \frac{4\pi}{k^2} \right) \left( \frac{2}{\pi r_c^2} \exp \left[ -\frac{2(\mathbf{r}_1 - \mathbf{r}_2)^2}{r_c^2} \right] \right), \quad (2.16)$$

where  $r_c$  is a measure of the phase correlation length of the target's surface. Here, we assume diffuse reflection only. In particular, we assume that there is no specular component in the reflected field (this is equivalent to assuming that the reflected optical phase variance  $\sigma_\phi^2 \gg 1$  (see Appendix A). Hence, the reflected field obeys circular complex Gaussian statistics.<sup>8</sup> In Appendix B, we present general expressions for the covariance when the magnitude of the reflection coefficient varies spatially. In the limit of complete spatial incoherence (i.e.,  $r_c \rightarrow 0$ ), we have  $B_\psi \rightarrow (4\pi/k^2)\delta(\mathbf{r}_1 - \mathbf{r}_2)$ , where  $\delta(\mathbf{r})$  is the Dirac delta-function. That is, for fully developed speckle, the reflected optical phase function is completely random and delta correlated. For a

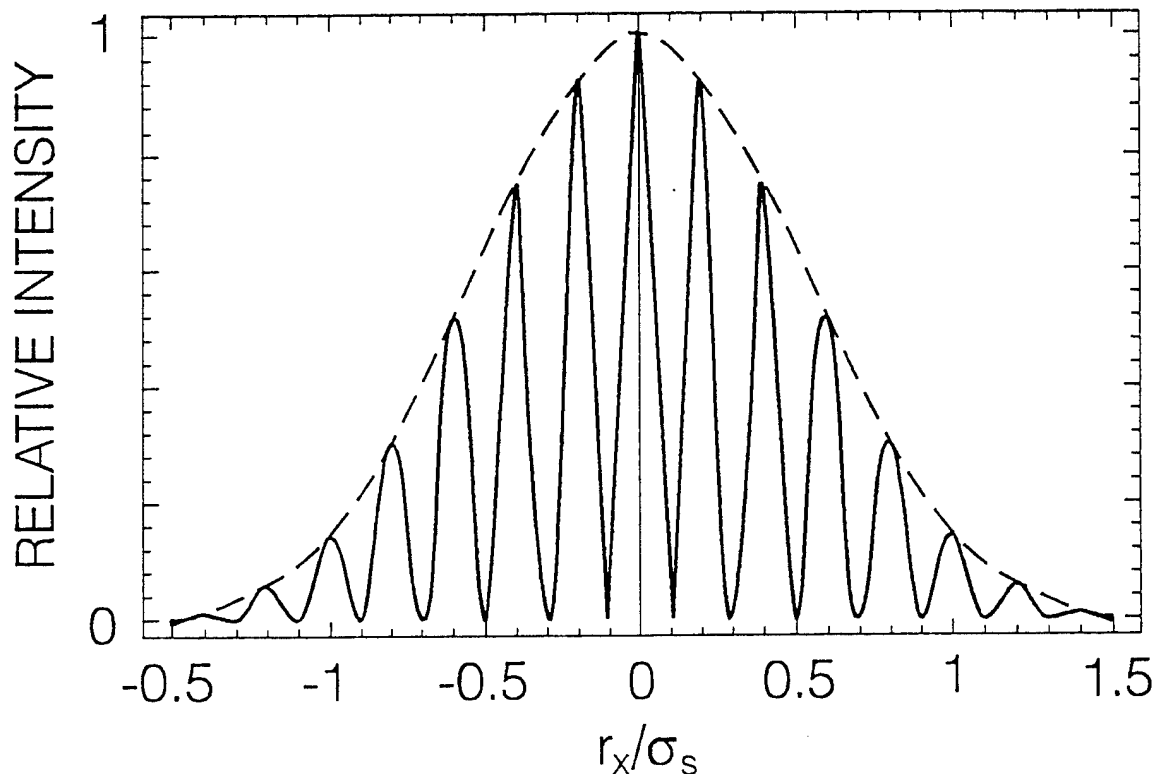


Figure 3. The reflected intensity distribution for  $\Lambda = \sigma_s/5$ .

diffuser moving with a constant velocity,  $\mathbf{v}$ , we assume that the time evolution of the reflected phase is given by

$$\psi(\mathbf{r}, t + \tau) = \psi(\mathbf{r} - \mathbf{v}\tau, t) \quad (2.17)$$

That is, the reflected phase at any position in a coordinate system moving along with the diffuser does not change in time (i.e., a Taylor's hypothesis).

On substituting Eqs. (2.2) and (2.5) into Eq. (2.1), we obtain from the first term on the right-hand side of Eq. (2.1) a term of the form

$$\left\langle U_o(\mathbf{r}_1, t) U_o^*(\mathbf{r}_2', t + \tau) U_o^*(\mathbf{r}_2, t) U_o(\mathbf{r}_1', t + \tau) \right\rangle, \quad (2.18)$$

where  $\mathbf{r}_1$ ,  $\mathbf{r}_1'$ ,  $\mathbf{r}_2$ , and  $\mathbf{r}_2'$  are integration variables that result when the substitutions alluded to above are carried out. In order to perform the statistical average over the four indicated reflected fields, we invoke the circular complex Gaussian statistics of the underlying speckle fields to write the average implied by expression (2.18) as

$$\begin{aligned} & \left\langle U_o(\mathbf{r}_1, t) U_o^*(\mathbf{r}_2', t + \tau) U_o^*(\mathbf{r}_2, t) U_o(\mathbf{r}_1', t + \tau) \right\rangle = \\ & \left\langle U_o(\mathbf{r}_1, t) U_o^*(\mathbf{r}_2, t) \right\rangle \left\langle U_o^*(\mathbf{r}_2', t + \tau) U_o(\mathbf{r}_1', t + \tau) \right\rangle \\ & + \left\langle U_o(\mathbf{r}_1, t) U_o^*(\mathbf{r}_2', t + \tau) \right\rangle \left\langle U_o^*(\mathbf{r}_2, t) U_o(\mathbf{r}_1', t + \tau) \right\rangle. \end{aligned} \quad (2.19)$$

From the discussion preceding Eq. (2.17), it is easily seen that the first term on the right-hand side of Eq. (2.19) will yield an expression that is identically canceled by the second term on the right side of Eq. (2.1). As a result, we obtain

$$C_i(\tau) = \int d\mathbf{p}_1 W(\mathbf{p}_1) \int d\mathbf{p}_2 W(\mathbf{p}_2) K(\mathbf{p}_1, \mathbf{p}_2; \tau), \quad (2.20)$$

where

$$\begin{aligned}
K(\mathbf{p}_1, \mathbf{p}_2; \tau) = & \int d\mathbf{r}_1 \int d\mathbf{r}_2 \int d\mathbf{r}_1' \int d\mathbf{r}_2' \\
& \times G(\mathbf{r}_1, \mathbf{p}_1) G^*(\mathbf{r}_2, \mathbf{p}_2) G(\mathbf{r}_1', \mathbf{p}_2) G^*(\mathbf{r}_2', \mathbf{p}_2) \\
& \times \langle U_o(\mathbf{r}_1, t) U_o^*(\mathbf{r}_2', t + \tau) \rangle \\
& \times \langle U_o^*(\mathbf{r}_2, t) U_o(\mathbf{r}_1', t + \tau) \rangle.
\end{aligned} \tag{2.21}$$

By employing Eqs. (2.13)–(2.17), we obtain that

$$K(\mathbf{p}_1, \mathbf{p}_2; \tau) = \left| \int d\mathbf{r}_1 U_i(\mathbf{r}_1) G(\mathbf{r}_1, \mathbf{p}_1) \int d\mathbf{r}_2 U_i^*(\mathbf{r}_2) G^*(\mathbf{r}_2, \mathbf{p}_2) B_\psi(\mathbf{r}_1, \mathbf{r}_2 \tau) \right|^2, \tag{2.22}$$

where

$$\mathbf{r}_{2\tau} = \mathbf{r}_2 + \mathbf{v}\tau. \tag{2.23}$$

Substituting Eqs. (2.10), (2.14), (2.16), and (2.22) into Eq. (2.20) yields an integral whose integrand contains multiplicative factors of the form  $\cos(\kappa_x r_{1x}) \cos(\kappa_x r_{2\tau x})$ , which when expanded, produce additive terms of the form  $\exp[\pm i\kappa_x(r_{1x} + r_{2x} + v_x \tau)]$  (the direct terms), and  $\exp[\pm i\kappa_x v_x \tau]$  (the cross terms). It can be shown that the direct terms yield, after performing the integrations over object space, multiplicative factors of the form  $\exp[-c(\kappa_x \sigma_s)^2]$ , where  $c$  is a dimensionless constant of the order unity. Because we assume that there are many fringes contained within the reflected spot,  $\kappa_x \sigma_s = 2\pi\sigma_s / \Lambda \gg 1$  and hence, the contribution of the direct terms to the covariance are negligible. On the other hand, it can be shown that because the cross terms are independent of object space coordinates they yield an overall multiplicative factor to the covariance that equals  $\cos^2(\kappa_x v_x \tau / 2) = [1 + \cos(\kappa_x v_x \tau)] / 2$ .

The resulting integration's have been performed using the *Mathematica* computer program,<sup>9</sup> with the final result that

$$C_i(\tau) = \frac{\langle i \rangle^2}{N} \left( \frac{1 + \cos(\kappa_x v_x \tau)}{2} \right) \exp \left( - \frac{(v\tau)^2}{\sigma_s^2 + r_c^2} \right), \tag{2.24}$$

where the mean current,  $\langle i \rangle = \langle i(t) \rangle = \langle i(t + \tau) \rangle$ , is given by

$$\begin{aligned}
\langle i \rangle &= \int d\mathbf{p} W(\mathbf{p}) \int d\mathbf{r}_1 \int d\mathbf{r}_2 B_\psi(\mathbf{r}_1, \mathbf{r}_2) U_i(\mathbf{r}_1) U_i^*(\mathbf{r}_2) G(\mathbf{r}_1, \mathbf{p}) G^*(\mathbf{r}_2, \mathbf{p}) \\
&= \alpha P_o \left( \frac{\sigma}{2f_1} \right)^2 \frac{1}{1 + \frac{r_c^2}{\omega^2} + \frac{r_c^2}{\sigma_s^2}}, \tag{2.25}
\end{aligned}$$

and  $N$ , the number of independent modes that pass through the optical system to the measurement aperture, is given by<sup>6</sup>

$$N = \frac{\left( 1 + \frac{\sigma_s^2}{\omega^2} \right) \left( 1 + \frac{r_c^2}{\sigma_s^2} \right)}{1 + \frac{r_c^2}{\omega^2} + \frac{r_c^2}{\sigma_s^2}}. \tag{2.26}$$

Equation (2.24) expresses the LDV covariance of photocurrent as a function of the phase correlation scale,  $r_c$ , for a planar diffuse reflecting target. To the best of our knowledge, this is the first analytical model that includes partial coherence of the target for LDV systems.

Examination of Eq. (2.24) reveals that the effect of partial coherence of the target's surface is to increase the effective size of the measurement (target) area. As a result, it can be shown that, for a sufficiently large signal-to-noise ratio, the number of observable oscillations in  $C_i(\tau)$  increases with increasing  $r_c$ , hence, increasing the sensitivity of the system. In the limit  $r_c \rightarrow 0$  (i.e., fully developed speckle), the results expressed in Eqs. (2.24)–(2.26) are identical to that obtained by Lading and Edwards.<sup>5</sup> On the other hand, for complete coherent reflection ( $r_c \rightarrow \infty$ ), examination of Eq. (2.25) yields that  $\langle i \rangle \rightarrow 0$ , as expected physically. This occurs because, for complete coherent reflection (i.e., specular reflection), there is no diffuse component of the photodetector current. Thus, for specular reflection, the LDV covariance of photocurrent is identically zero.

## 2.2 Rotating Targets

In this section, we consider, as indicated in Figure 4, a rotating shaft of radius  $R$  that has a surface that reflects light with complete incoherence (i.e.,  $r_c \rightarrow 0$ ). In all cases of interest, the maximum time-lag,  $\tau$ , and rotational velocity are sufficiently small such that the angular separation between a point on the surface at time  $t$ , and the corresponding point at time  $t + \tau$  is much less than unity. This is equivalent to the condition that the reflected spot size is small compared to the radius of the shaft (i.e.,  $\sigma_s/R \ll 1$ ), a condition that is always met in practice. For completeness, as discussed in the Introduction, we consider a finite receiver aperture, whose weighting function is given by Eq. (2.4). We then assume that the angular velocity of the shaft is parallel to the  $r_y$ -axis.

Assuming that the laser beams are normally incident on the target, the reflected optical field,  $U_i(\mathbf{r})$  in the initial plane (i.e.,  $z = 0$ ) at the coordinate  $\{r_x, r_y, 0\}$  contains the multiplicative factor  $\exp(2ikbr_x^2)$ ,<sup>10</sup> where

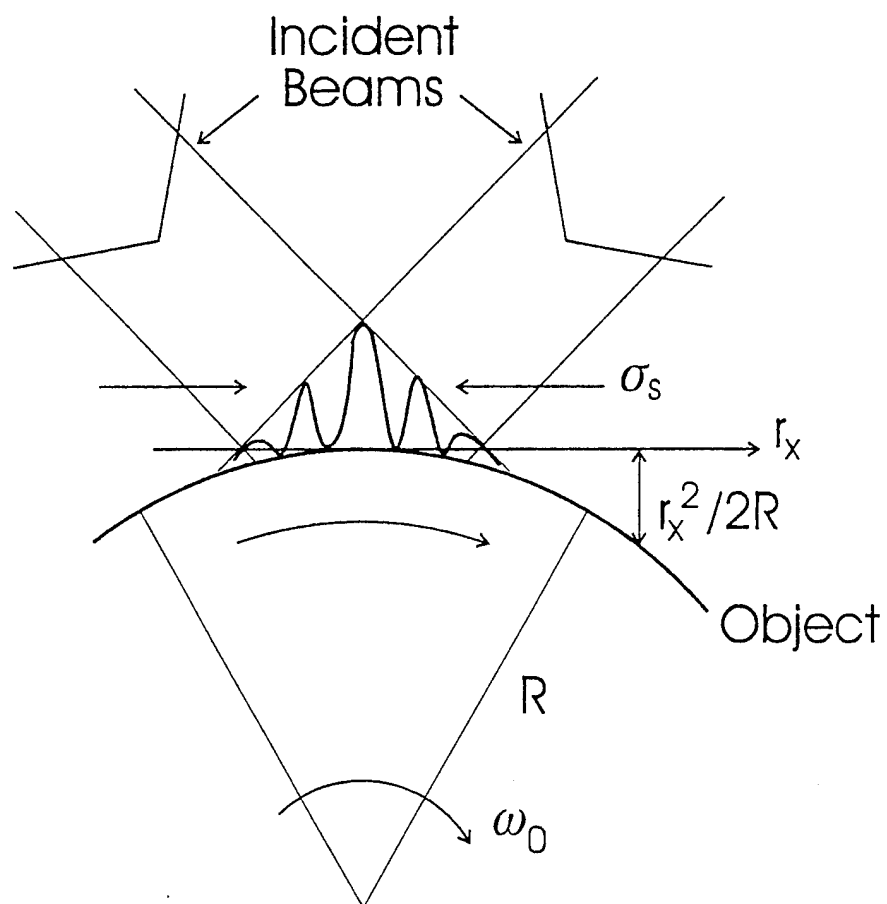


Figure 4. Measurement geometry for a rotating cylindrical shaft.

$$b = \frac{1}{2R}. \quad (2.27)$$

That is, Eq (2.13) becomes:

$$U_o(\mathbf{r}, t) = U_i(\mathbf{r}) \exp(2ikbr_x^2) \psi(\mathbf{r}, t). \quad (2.28)$$

In this case, it can be shown by methods similar to that in obtaining Eq. (2.24) that the covariance of the photocurrent, in the presence of a rotating shaft and a finite detector measurement aperture,  $\sigma_a$  is given by

$$C_i(\tau) = \frac{\langle i \rangle^2}{N} \left( \frac{1 + \cos(\kappa_x \omega_o R \tau)}{2} \right) \exp \left[ -\frac{(\omega_o R \tau)^2}{\Delta^2} \right], \quad (2.29)$$

where  $w_o$  is the magnitude of the angular velocity of the rotating shaft,

$$\frac{1}{\Delta^2} = \frac{1}{\sigma_s^2} + \frac{1}{\omega^2 + \sigma_o^2} + \frac{(k\sigma_s \omega / R)^2}{\sigma_s^2 + \omega^2}, \quad (2.30)$$

$$\langle i \rangle = \alpha P_o \left( \frac{\sigma}{2f_1} \right)^2 \frac{1}{1 + (\omega_s^2 / \sigma_a^2)}, \quad (2.31)$$

$$N = N_c \left( \frac{\omega^2 + \sigma_o^2}{(\omega_s / m)^2 + \sigma_o^2} \right)^{1/2}, \quad (2.32)$$

$$N_c = 1 + \left( \frac{\sigma_s}{\omega} \right)^2 = 1 + \left( \frac{k\sigma\sigma_s}{2f_1} \right)^2, \quad (2.33)$$

$$\omega_s^2 = (m\sigma_s)^2 + \left( \frac{2f_2}{k\sigma} \right)^2, \quad (2.34)$$

and

$$\sigma_o = \frac{\sigma_a}{m}. \quad (2.35)$$

The quantities  $N$ ,  $N_c$ ,  $w_s$ , and  $s_o$  are, respectively, the number of independent (optical) modes that passes through the measurement aperture to the detector plane, the corresponding number of modes captured by the optical system, the  $1/e^2$  radius of the image of the reflected spot, and the detector aperture radius referred to object-space coordinates.<sup>3</sup> Note, in contrast to the planar case, interference effects due to the presence of the curved target cause a reduction in the temporal width of the covariance. Physically, this arises due to destructive interference, which reduces the effective imaged spot size and, hence, a shorter corresponding transit time is obtained.

For detector apertures that are large compared with the size of the imaged spot, Eq. (2.29) becomes



$$C_i(\tau) = \frac{\langle i \rangle^2}{N_c} \left( \frac{1 + \cos(\kappa_x \omega_o R \tau)}{2} \right) \exp \left[ - \left( \frac{\omega_o R \tau}{\sigma_s} \right)^2 \left( 1 + \frac{(k \sigma_s \omega / R)^2}{1 + \frac{\omega^2}{\sigma_s^2}} \right) \right] \quad (\sigma_a \rightarrow \infty), \quad (2.36)$$

where  $\langle i \rangle$  and  $N_c$  are given by Eqs. (2.31) (with  $\sigma_a \rightarrow \infty$ ) and (2.33), respectively.

As indicated above, the presence of the curved target causes a reduction in the temporal width of the covariance. For simplicity, consider the case of large detector apertures, which applies for almost all systems of practical concern. Then, examination of Eq. (2.36) reveals that the effects of rotation become significant for  $R < R_{min}$ , where  $R_{min}$  is determined from the condition that

$$\frac{(k \omega \sigma_s / R_{min})^2}{1 + \frac{\omega^2}{\sigma_s^2}} > 1. \quad (2.37)$$

For example, for  $\omega \ll \sigma_s$ , (i.e.,  $N \gg 1$ ) Eq. (2.37) yields that

$$R_{min} = k \omega \sigma_s, \quad (2.38)$$

while for  $\omega \gg \sigma_s$ , (i.e.,  $N \cong 1$ ) we obtain that

$$R_{min} = k \sigma_s^2. \quad (2.39)$$

### 3. Error Estimates

Of primary concern in LDV measurements is the determination of the velocity of a target. Because the current covariance is an oscillating function of the time-lag  $\tau$ , velocity information is difficult to obtain directly from the covariance. However, the corresponding power spectrum is a peaked function, from which velocity information can be extracted directly from knowledge of the location of the peak. Therefore, consider the autospectral density function of the covariance of photodetector current, defined as

$$S(f) = \int_{-\infty}^{\infty} C_i(\tau) e^{-2\pi i f \tau} d\tau, \quad (3.1)$$

where  $C_i(\tau)$  is given by Eqs. (2.24) and (2.29), and  $f$  denotes temporal frequency. Substituting either Eq. (2.24) or Eq. (2.29) into Eq. (3.1) yields a spectrum in the region of positive frequencies, near the peak, of the form (excluding the low-frequency region, i.e., the pedestal term)

$$S(f) = \frac{\langle i \rangle^2}{2\sqrt{\pi} \Delta f N} \exp \left[ -\frac{(f - f_o)^2}{\Delta f^2} \right], \quad (3.2)$$

where

$$f_o = \begin{cases} v_x / \Lambda & \text{(planar targets)} \\ \omega_o R / \Lambda & \text{(rotating targets)} \end{cases}, \quad (3.3)$$

and

$$\Delta f = \begin{cases} v / \pi \sqrt{\sigma_s^2 + r_c^2} & \text{(planar targets)} \\ \omega_o R / \pi \Delta & \text{(rotating targets)} \end{cases}, \quad (3.4)$$

In general, in contrast to planar targets, the effects of curved targets results in an increase in the spectral width,  $\Delta f$  [see Eq. (2.30)]. Note, in particular, that if one knew the precise location of the peak,  $f_o$ , the corresponding velocity information follows directly from Eq. (3.3). We next present expressions that indicate how well one can estimate the exact location of the peak of the power spectrum in practice.

For  $f \neq 0$ , the variance of the estimate of the autospectral density,  $\hat{S}(f)$ , is given by<sup>11</sup>

$$\begin{aligned} \text{Var}[\hat{S}(f)] &= \left\langle \left( \hat{S}(f) - \langle \hat{S}(f) \rangle \right)^2 \right\rangle \\ &= \frac{S^2(f)}{B_e T}, \end{aligned} \quad (3.5)$$

where  $T$  is the finite record length, and  $B_e$  is the resolution bandwidth centered at frequency  $f$  (see Sec. 8.5 of Ref. 11). The results given in Eq. (3.5) are based on the assumption that the filtered data behave like bandwidth-limited Gaussian white noise. This is an excellent assumption in practice when the filter resolution bandwidth,  $B_e$ , is sufficiently small. The central limit theorem applies to indicate that the filtered data should be more Gaussian than the input data, and the fact that  $B_e$  is small means that the output spectrum must be essentially constant.

In order to obtain an estimate for the error in determining the precise location of the peak of autospectral density function, we expand  $S(f)$  near  $f = f_o$ , which yields the estimate

$$\hat{S}(f) = \left[ 1 - \frac{(f - f_o)^2}{\Delta f^2} \right] S(f_o). \quad (3.6)$$

Thus, in terms of estimates of  $f$  near  $f_o$ ,  $\text{Var}[\hat{S}(f)]$  is given by

$$\text{Var}[\hat{S}(f)] = \frac{\langle (f - f_o)^4 \rangle}{\Delta f^4} S(f_o)^2. \quad (3.7)$$

Assume next that these values of  $f$  are such that  $f$  follows a normal distribution with  $\langle f \rangle = f_o$ , and variance  $\sigma_{f_o}^2$ . Then, the fourth moment in Eq. (3.7) is equal to  $3\sigma_{f_o}^4$ , from which it follows that the variance of the estimate of the location of the peak in the autospectral density function is given by

$$\sigma_{f_o}^2 = \sqrt{1/3} \Delta f^2 \text{Var}[\hat{S}(f_o)]^{1/2} / S(f_o). \quad (3.8)$$

Substituting Eq. (3.2) into Eq. (3.8) yields that

$$\sigma_{f_o}^2 = \frac{\Delta f^2}{\sqrt{3B_e T}}. \quad (3.9)$$

On the basis of the normal distribution and Eq. (3.9), one can obtain a confidence interval for the unknown true value of  $f_o$ , in terms of system parameters, based on any single estimate,  $\hat{f}$ . Thus, for example, the 95% confidence interval for determining the location of the peak of the spectrum is  $f = f_o \pm 2\sigma_{f_o}$ .

## 4. Discussion and Conclusion

Based on the results obtained in this report for LDV systems and the corresponding results obtained in a previous article<sup>2</sup> treating the Laser-Time-of Flight velocimeter (LTV), a comparison between the two systems can be made. We consider both results relating to measurements on targets giving rise to fully developed speckle fields. To compare the two systems, the transmitters for the two systems are assumed to have the same numerical apertures, which make the number of fringes in the LDV system,  $N_f$ , equal to the relative distance between the focused spots divided by the spot radius in the LTV system. Further, the numerical apertures of the detector systems are assumed identical. The comparison is made with respect to the error estimates, the minimum shaft radius, and the effect of velocity misalignment.

Equation 57 of Ref. 2 gives the variance of the estimated value of the location of the peak of the cross covariance, which can be easily converted to give the normalized variance for estimating the velocity in a LTV system:

$$\frac{s_v^2}{v^2} \propto \frac{1}{N_f^2 \sqrt{B_e T}}, \quad (4.1)$$

where the bandwidth for the LTV signal is determined by the effective transit time through one of the illuminated spots, i.e.,

$$B_e = v \left( \frac{1}{\sigma_s^2} + \frac{1}{\omega^2} \right)^{1/2}, \quad (4.2)$$

for the case of large detector apertures. The corresponding normalized variance for the LDV system, as obtained from Eq. (3.9), is

$$\frac{\sigma_v^2}{v^2} \propto \frac{1}{N_f^2 \sqrt{B_e T}} \left( \frac{v_x}{v} \right)^2, \quad (4.3)$$

where the spectral bandwidth, for the case of large detector apertures, is also given by Eq. (4.2). Comparing the functional dependence of the normalized variances, Eqs. (4.1) and (4.3), reveals that we arrive at identical *expressions* if the velocity in the LDV system is perpendicular to the fringes. Note that the bandwidth,  $B_e$ , is different for the two systems. The LTV system has a bandwidth that is given by the transit time through one of the focused spots, whereas the LDV system has a corresponding bandwidth determined by the transit time (which is a factor  $N_f$  larger) through the entire fringe pattern. Comparing Eqs. (4.1) and (4.3), it follows that the variance of the estimated velocity is, therefore, a factor  $N_f^{1/2}$  smaller for the LTV system in comparison to

the LDV system. We note that neither Eq. (4.1) or (4.3) represents fundamental limits,<sup>5</sup> but even taking the detailed signal statistics into consideration the conclusion appears to be valid.

Furthermore, the number of collected modes, Eq. (2.33), is determined by the spot size for the LTV system and by the size of the fringe pattern for the LDV system. Identical conditions for the detector and transmitter set-ups, therefore, result in a higher normalized time-lagged auto covariance for the LTV system. In these respects, the LTV system is superior to the LDV system. A decrease in resolution is expected for variations from optimum alignment for the LDV system, whereas the basic LTV system with circular spots in the measuring volume will lose signal in this case.

The minimum radii of curvature for the two systems are summarized in Table 1. Identical performance is obtained if the distance between the spots in the LTV system equals the spot size in the LDV system. Both LDV and LTV systems will suffer a decrease in the magnitude of the cross covariance and auto covariance as the target diameter decreases, while the temporal widths of the respective covariances increase correspondingly with decreasing values of the spot size.

Finite spatial coherence of the reflecting target has been considered for the LDV system only, showing an apparent increase [see Eq. (2.24)] of the measuring volume, yielding a decrease in the variance of the estimated velocity. Further, this is accompanied by a decrease in the number of optical modes,  $N$ , and therefore an increase in the normalized auto covariance and a slight decrease in the magnitude of the detected signal. Targets giving rise to fully developed speckle will, for both systems, yield normalized covariance functions that are inversely proportional to the number of modes collected by the receiver.

The method of  $ABCD$  matrices has been applied to the analysis of LDV systems in conjunction with targets having correlated surface structures. This method is based on the assumption that all apertures are of Gaussian shape. The resulting Huygens-Fresnel integrals can then be solved analytically, whereby later mathematical approximations can be avoided. The auto covariance and power spectrum have been obtained in closed analytical form, which provides a tool for parametric optimization of the optical system. System performance has been analyzed in that the variance of the estimated velocity has been obtained in terms relating to the optical system and the target surface reflectance characteristics. Further, measurement restrictions for cylindrical rotating targets have been obtained, and the results have been compared with previous results for time-of flight velocimetry.

Table 1. Minimum Radii of Curvature for Measurement on Cylindrical Surfaces in the Two Limiting Cases for LDV and LTV

Minimum Radius of Curvature	Time of Flight Velocimetry	Laser-Doppler Velocimetry
$\omega < \sigma_s$	$2kd\omega$	$k\omega\sigma_s$
$\omega > \sigma_s$	$2kd\sigma_s$	$k\sigma_s^2$

## References and Notes

1. L. E. Drain, *The Laser Doppler Technique* (Wiley, Chichester 1980).
2. L. Lading, "Principles of Laser Anemometry" in *Optical Diagnostics for Flow Processes* (Eds. L. Lading, P. Buchhave, and G. Wigley, Plenum, New York 1994) pp. 85-125.
3. H. T. Yura, S. G. Hanson, and T. P. Grum, *Speckle: statistics and interferometric decorrelation effects in complex ABCD optical systems*, Jr. Opt. Soc. Am. A, **10**, 316-323, (1993).
4. R.V. Edwards, J. C. Angus, and J. W. Dunning, "Spectral analysis of the signal from a laser Doppler flowmeter: time independent systems", J. Appl. Phys. **42**, 837-850 (1971) and W. K. George and J. L. Lumley, "The laser Doppler velocimeter and its application to the measurement of turbulence", J. Fluid Mech. **60**, 312-362 (1973).
5. L. Lading and R. V. Edwards, *Laser velocimeters: lower limits to uncertainty*, Appl. Opt. **32**, 3855-3866 (1993).
6. H. T. Yura and S.G. Hanson, *Laser-time-of-flight velocimetry: analytical solution to the of the optical system based on ABCD matrices*, Jr. Opt. Soc. Am. A, Vol. **10**, 1918-1924 (1993).
7. A. E. Siegman, *Lasers* (University Science Books, Mill Valley, Calif. 1986), Chap. 20.
8. J. W. Goodman, *LASER SPECKLE and Related Phenomena*, Editor: J. C. Dainty, Chap. 2, Springer-Verlag, Berlin, 1984.
9. S. Wolfram, *Mathematica A System for Doing Mathematics by Computer*, (Addison-Wesley Publishing Co., Redwood City California, 1991).
10. For non-normal angles of incidence, the factor of 2 in the exponent is replaced by  $(1+\cos\beta)$ , where  $\beta$  is the angle between the direction of propagation and the normal to the surface.
11. J. S. Bendat and A. G. Piersol, *Random Data: Analyses and Measurement Procedures* (Wiley, New York, 1986), Chap. 8.

## Appendix A

In this Appendix, we present a physical model that relates the complex reflection coefficient to the surface height fluctuations. Following Goodman,<sup>8</sup> we adopt an elementary relation that leads to tractable results, which is often used in analysis and is reasonably accurate if the surface slopes are small. In particular, we express the reflection coefficient as [see Eq. (2.162) and Fig. 2.23 of Ref.8]

$$\psi(\mathbf{r}) = |\psi(\mathbf{r})| \exp[i\phi(\mathbf{r})] \quad (\text{A-1})$$

where,

$$\phi(\mathbf{r}) = k(1 + \cos\beta)h(\mathbf{r}), \quad (\text{A-2})$$

$h(\mathbf{r})$  is the surface fluctuation in surface heights,  $\beta$  is the angle between the direction of propagation of the laser beams and the normal to the surface, and, for simplicity in notation, we have suppressed the explicit dependence on time. Because it is assumed that  $h(\mathbf{r})$  is a zero-mean wide-sense stationary random process, so too is the phase angle  $\phi(\mathbf{r})$ . If  $\sigma_h^2$  represents the variance of  $h$ , then the variance of  $\phi$  is given by

$$\sigma_\phi^2 = [k(1 + \cos\beta)\sigma_h]^2. \quad (\text{A-3})$$

Assuming that  $|\psi(\mathbf{r})| = 1$ , and that the surface height fluctuations are a Gaussian random process, the correlation function  $B_\psi(\mathbf{r}_1, \mathbf{r}_2) = \langle \psi(\mathbf{r}_1)\psi^*(\mathbf{r}_2) \rangle$  can be expressed as

$$\begin{aligned} B_\psi(\mathbf{r}_1, \mathbf{r}_2) &= \langle \exp[i(\phi(\mathbf{r}_1) - \phi(\mathbf{r}_2))] \rangle \\ &= \exp[-\sigma_\phi^2(1 - b_h(\mathbf{r}_1, \mathbf{r}_2))], \end{aligned} \quad (\text{A-4})$$

where  $b_h$  is the normalized correlation function of the surface height fluctuations.

Equation (A-4) provides us with a specific relationship between the correlation properties of the reflection coefficient and the correlation properties of the reflecting surface. To proceed further, we assume that the statistics of the reflecting surface are stationary and that the normalized correlation function of the surface heights is also of Gaussian form,

$$b_h(r) = \exp\left[-2\left(\frac{r}{r_h}\right)^2\right], \quad (\text{A-5})$$

where  $r = |\mathbf{r}_1 - \mathbf{r}_2|$ , and  $r_h$  is the lateral coherence length of the surface heights fluctuations. Hence, the correlation function  $B_\psi$  becomes

$$B_\psi(r) = \exp\left[-\sigma_\phi^2\left(1 - e^{-2(r/r_h)^2}\right)\right]. \quad (\text{A-6})$$

For almost all cases of practical concern, the phase variance  $\sigma_\phi^2$  is greater than unity and hence,  $B_\psi$  can be expressed as

$$B_\psi(r) = \exp\left[-2\left(\frac{r}{r_c}\right)^2\right], \quad (\text{A-7})$$

where

$$r_c = \frac{r_h}{\sigma_\phi} = \frac{r_h}{k(1 + \cos\beta)\sigma_h}. \quad (\text{A-8})$$

is the phase lateral coherence length.

For mathematical convenience, we want to use a correlation function that becomes a Dirac delta function in the limit of complete incoherent reflection. That is, for fully developed speckle, we require that  $B_\psi(\mathbf{r}_1, \mathbf{r}_2) = a\delta(\mathbf{r}_1 - \mathbf{r}_2)$ , where  $a$  is a constant that is *independent* of the optical system. The quantity  $a$  can be determined from the requirement that the mean reflected radiance of fully developed speckle is given by  $I_o\rho A/\pi$ , where  $I_o$  is the incident intensity,  $\rho$  is the reflection coefficient, and  $A$  is the area of the illuminated spot (i.e., Lambert's law). Hence, it can be shown that  $a = 4\pi/k^2$ . Based on these considerations and Eq. (A-7), we use a correlation function for partial coherent diffuse reflection given by

$$B_\psi(\mathbf{r}_1, \mathbf{r}_2) = \left(\frac{4\pi}{k^2}\right) \left(\frac{2}{\pi r_c^2} \exp\left[-\frac{2(\mathbf{r}_1 - \mathbf{r}_2)^2}{r_c^2}\right]\right). \quad (\text{A-9})$$

Note, in the limit  $r_c \rightarrow 0$ , we have from Eq. (A-9) that  $B_\psi \rightarrow (4\pi/k^2)\delta(\mathbf{r}_1 - \mathbf{r}_2)$ .



## Appendix B

In this Appendix, we now assume that the magnitude of the reflection coefficient exhibits deterministic spatial variations over dimensions of the reflected laser spot. Specifically, we assume that

$$|\psi(\mathbf{r}, t)| = \sqrt{\rho(\mathbf{r}, t)}, \quad (\text{B-1})$$

where  $\rho(\mathbf{r}, t)$  is the magnitude of the reflection coefficient. Then, following similar arguments that led to Eq. (2.22), it is straightforward to show that Eq. (2.22) becomes

$$K(\mathbf{p}_1, \mathbf{p}_2; \tau) = \left| \int d\mathbf{r}_1 \rho(\mathbf{r}_1)^{1/2} U_i(\mathbf{r}_1) G(\mathbf{r}_1, \mathbf{p}_1) \int d\mathbf{r}_2 \rho(\mathbf{r}_2)^{1/2} U_i^*(\mathbf{r}_2) G^*(\mathbf{r}_2, \mathbf{p}_2) B_\psi(\mathbf{r}_1, \mathbf{r}_2, \tau) \right|^2. \quad (\text{B-2})$$

For the special case of fully developed speckle (i.e.,  $B_\psi(\mathbf{r}_1, \mathbf{r}_2, \tau) = (4\pi/k^2) \delta(\mathbf{r}_1 - \mathbf{r}_2 - \mathbf{v}\tau)$ ), Eq. (B-2) becomes

$$K(\mathbf{p}_1, \mathbf{p}_2; \tau) = \left| \frac{4\pi}{k^2} \int d\mathbf{r} \sqrt{\rho(\mathbf{r}) \rho(\mathbf{r}_\tau)} U_i(\mathbf{r}) U_i^*(\mathbf{r}_\tau) G(\mathbf{r}, \mathbf{p}_1) G^*(\mathbf{r}_\tau, \mathbf{p}_2) \right|^2. \quad (\text{B-3})$$

where

$$\mathbf{r}_\tau = \mathbf{r} + \mathbf{v}\tau. \quad (\text{B-4})$$

## TECHNOLOGY OPERATIONS

The Aerospace Corporation functions as an "architect-engineer" for national security programs, specializing in advanced military space systems. The Corporation's Technology Operations supports the effective and timely development and operation of national security systems through scientific research and the application of advanced technology. Vital to the success of the Corporation is the technical staff's wide-ranging expertise and its ability to stay abreast of new technological developments and program support issues associated with rapidly evolving space systems. Contributing capabilities are provided by these individual Technology Centers:

**Electronics Technology Center:** Microelectronics, VLSI reliability, failure analysis, solid-state device physics, compound semiconductors, radiation effects, infrared and CCD detector devices, Micro-Electro-Mechanical Systems (MEMS), and data storage and display technologies; lasers and electro-optics, solid state laser design, micro-optics, optical communications, and fiber optic sensors; atomic frequency standards, applied laser spectroscopy, laser chemistry, atmospheric propagation and beam control, LIDAR/LADAR remote sensing; solar cell and array testing and evaluation, battery electrochemistry, battery testing and evaluation.

**Mechanics and Materials Technology Center:** Evaluation and characterization of new materials: metals, alloys, ceramics, polymers and composites; development and analysis of advanced materials processing and deposition techniques; nondestructive evaluation, component failure analysis and reliability; fracture mechanics and stress corrosion; analysis and evaluation of materials at cryogenic and elevated temperatures; launch vehicle fluid mechanics, heat transfer and flight dynamics; aerothermodynamics; chemical and electric propulsion; environmental chemistry; combustion processes; spacecraft structural mechanics, space environment effects on materials, hardening and vulnerability assessment; contamination, thermal and structural control; lubrication and surface phenomena; microengineering technology and microinstrument development.

**Space and Environment Technology Center:** Magnetospheric, auroral and cosmic ray physics, wave-particle interactions, magnetospheric plasma waves; atmospheric and ionospheric physics, density and composition of the upper atmosphere, remote sensing using atmospheric radiation; solar physics, infrared astronomy, infrared signature analysis; effects of solar activity, magnetic storms and nuclear explosions on the earth's atmosphere, ionosphere and magnetosphere; effects of electromagnetic and particulate radiations on space systems; space instrumentation; propellant chemistry, chemical dynamics, environmental chemistry, trace detection; atmospheric chemical reactions, atmospheric optics, light scattering, state-specific chemical reactions and radiative signatures of missile plumes, and sensor out-of-field-of-view rejection.